Kakinuma Y et al
Figure 4

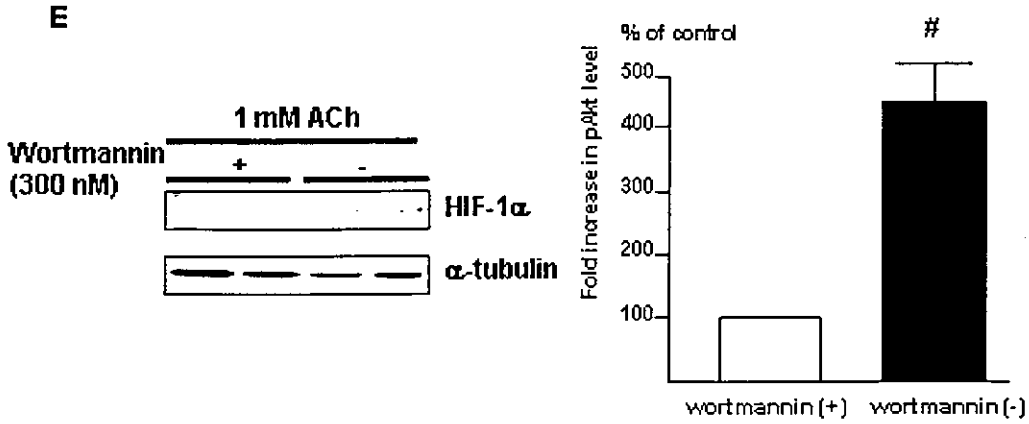

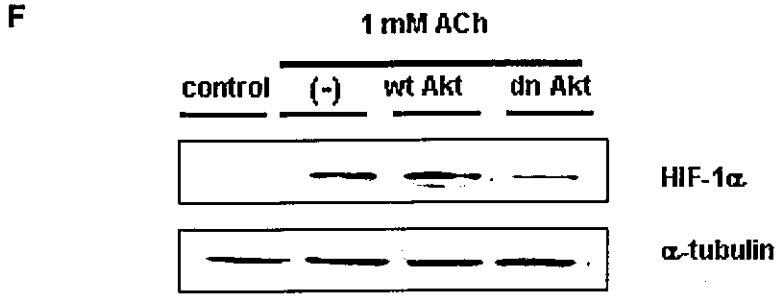

Figure 5

Kakinuma Y et al
Figure 5

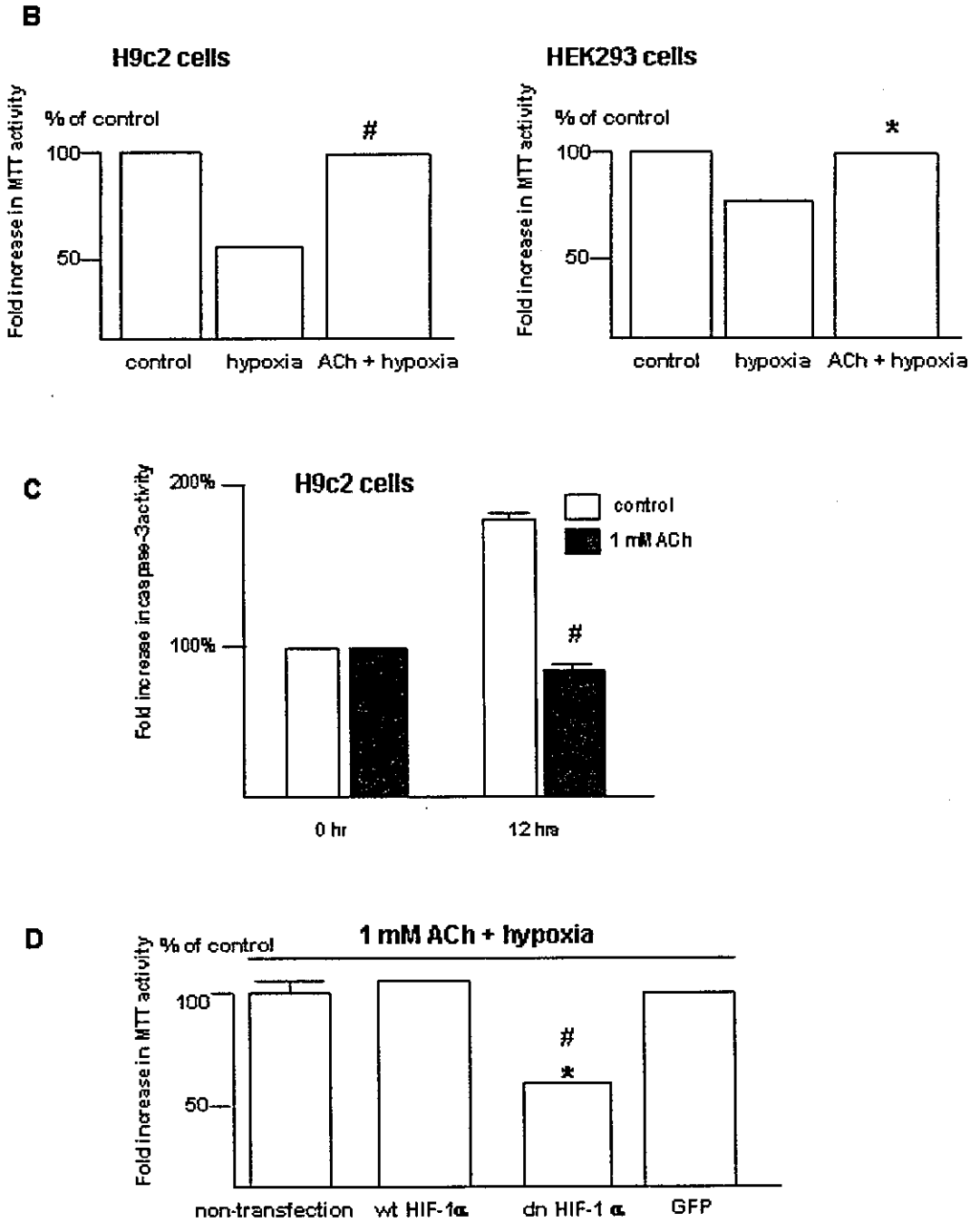

Kakinuma Y et al
Figure 6

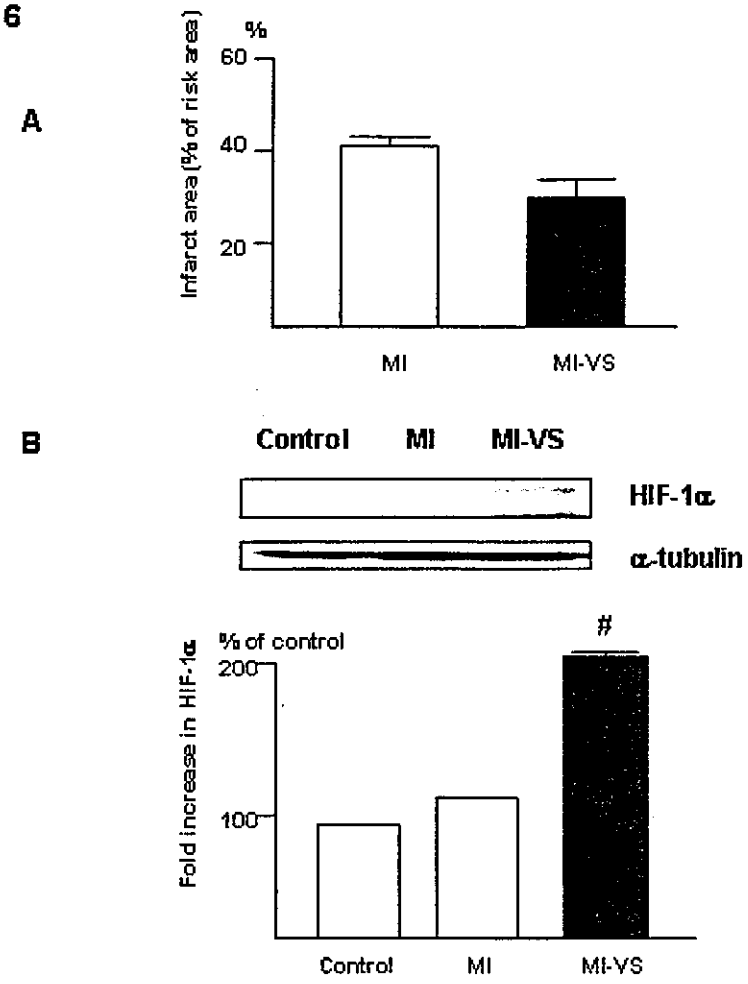

Figure 7

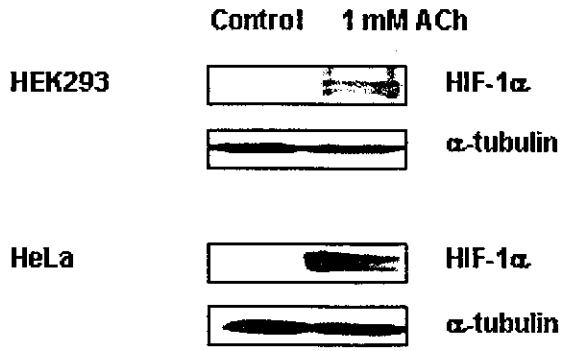

HIF-1α is Involved in the Attenuation of Experimentally Induced Rat Glomerulonephritis

Yoshihiro Kudo[1], Yoshihiko Kakinuma[2], Yasukiyo Mori[3], Norihito Morimoto[1], Takashi Karashima[4], Mutsuo Furihata[5], Takayuki Sato[2], Taro Shuin[4], Tetsuro Sugiura[1]

Departments of [1]Laboratory Medicine, [2]Cardiovascular Control, [4]Urology and [5] Tumor Pathology, Kochi Medical School, Kochi, Japan
[3]The Second Department of Internal Medicine, Kansai Medical University, Osaka, Japan

Address for Correspondence; Yoshihiko Kakinuma, M.D., Ph.D. Department of Cardiovascular Control, Kochi Medical School, Kochi 783-8505, Japan
Phone: +81-88-880-2311, Fax: +81-88-880-2310, E-mail: kakinuma@med.kochi-u.ac.jp

Abstract

Background/Aim: Among various kidney disease models, there are few rat glomerulonephritis (GN) models that develop in a short time, and with mainly glomerular lesions. Hypoxia-inducible factor (HIF)-1α is a transcriptional factor that induces genes supporting cell survival, but the involvement of HIF-1α in attenuating the progression of GN remains to be elucidated. We developed a new model of rat GN by co-administration of Angiotensin II (AII) with Habu snake venom (HV) and investigated whether HIF-1α is involved in renal protection. ***Methods:*** Male Wistar rats were unilaterally nephrectomized on day −1, and divided into 4 groups on day 0; N group (no treatment), HV group, A group (AII), and H+A group (HV and AII). To pre-induce HIF-1α, cobalt chloride ($CoCl_2$) was injected twice before injections of HV and AII in 11 rats.
Results: GN was detected only in the H+A group; observed first on day 2 and aggravated thereafter. HIF-1α was expressed in the glomeruli and renal tubules in the A and H+A groups. In the H+A group, GN was remarkably reduced by $CoCl_2$ pre-treatment (44.9% to 12.2%, $p<0.01$). ***Conclusion:*** Both HV and AII were critical for the development of GN, and HIF-1α remarkably attenuated the progression of GN.

Key Words

Glomerulonephritis, Habu snake venom, Angiotensin II, HIF-1α

Introduction

Many animal studies have been performed in attempts to overcome the poor prognosis of chronic renal failure due to diabetic nephropathy and glomerulonephritis (GN) [1-5]. Although factors involved in the pathogenesis of GN have been intensively investigated, the development of a proper animal GN model with high reproducibility and simplicity as well as a model without time-consuming process are required. Experimental rat models of GN are classified into several groups in terms of the pathophysiological mechanisms of renal diseases. Anti-glomerular basement membrane (GBM) nephritis was developed with depositions of immune complex using anti-glomerular basement membrane antibody [3,6], tubulo-interstitial injury was caused by cyclosporine A [4] and injury of renal tubules by ischemia [5]. However, there are few rat GN models with mainly pathological features in the glomeruli that are developed in a short time [7]. Angiotensin II (AII) is known to increase blood pressure through vascular contraction, and to be profoundly involved in vascular hypertrophy and the contraction of intrarenal arteries. AII is also directly involved in the progression of glomerulosclerosis via the effect of hyperfiltration with or without hypertension [8,9]. Many studies have revealed important factors involved in the pathogenesis of GN or factors aggravating GN, but evaluating further factors that suppress the occurrence of GN is also crucial. To investigate the features of renal protection, we focused on hypoxia-inducible factor (HIF)-1α. HIF-1α, a transcriptional factor with formation of a heterodimer with HIF-1β [10], is post-transcriptionally regulated and its protein level is elevated by hypoxia through inhibition of ubiquitin-mediated degradation. HIF-1α is known to be a survival factor responsible for inducing lines of genes supporting cell survival such as glucose metabolism (glucose transporters and glycolysis enzymes), vasomotor regulation (heme oxygenase-1 and endothelin-1), angiogenic growth (vascular endothelial growth factor), and anemia control (erythropoietin and transferrin) [11-13]. Recent studies have demonstrated that non-hypoxic stimuli like AII can also activate HIF-1α [14,15], but the role of HIF-1α induction in attenuating the progression of GN remains to be elucidated. Accordingly, we

developed a new rat GN model by co-administration of AII with Habu snake venom (HV) and investigated whether pre-induction of HIF-1α leads to renal protection.

Materials and Methods

Development of Rat GN Model

All experiments were approved by the institutional review board for the care of animal subjects and were performed in accordance with guidelines of Kochi Medical School. Nine-weeks old male Wistar rats (180-220g) were purchased from Japan SLC (Shizuoka, Japan). Rats were unilaterally nephrectomized on day -1. On day 0, the rats were divided into 4 groups. In the first group, no treatment was performed with any reagents or surgical procedure (N group, n=6). In the second group, rats were injected with 3.5 mg/kg of HV (Sigma-Aldrich Co., Steinheim, Germany) through the femoral vein (HV group, n=11). In the third group, rats were continuously administered with AII (100ng/min, Peptide Institute, Inc., Osaka, Japan) using Alzet osmotic pumps (DURECT Co., Cupertino, CA) (A group, n=11). In the fourth group, rats were administered with both HV and AII (H+A group, n=22). Rats were sacrificed on days 1, 2, 3 or 4, and kidneys excised for histochemical analysis (fig. 1).

Measurement of Systolic Blood Pressure

Systolic blood pressure (SBP) was measured by the tail-cuff method with an electro-sphygmomanometer (BP-98A, Softron Co., Tokyo, Japan). SBP was measured in conscious rats every day from day -1 to day 2. The SBP value for each rat was calculated as the average of 3 separate measurements at each session. SBP measurement was performed between 9 and 12 a.m. by a single blinded investigator.

Measurements of Serum Urea Nitrogen and Creatinine

Before the sacrifice, blood samples were obtained via an axillary vein for determination of serum urea nitrogen (UN) and creatinine (Cr) levels. Serum UN and Cr levels were determined enzymatically with automation-analysis equipment (Hitachi 7350, Hitachi Co., Ibaragi, Japan) in our laboratory center.

Histological Analysis

To evaluate the progression of GN in our animal model, histological analyses were performed using the periodic acid-Schiff (PAS) and periodic acid-methenamine silver (PAM) reagents. After the specimens were paraffin-embedded, 4-micrometer sectioned samples were stained with PAS and PAM reagents and counterstained with hematoxylin. For quantitative analysis, the ratio of damaged glomeruli to all glomeruli in the sectioned sample was calculated and the percentage of GN in the section was evaluated. Moreover, semiquantitative analysis was performed to evaluate more precisely the morphological changes of our GN model according to the protocol in previous studies [16,17]. A minimum of 20 glomeruli (ranging from 20 to 60 glomeruli) in each specimen were examined and the severity of the mesangiolysis lesion was graded from 0 to 4+ according to the percentage of glomerular involvement; a 1+ lesion represented an involvement of 25 % of the glomerulus while a 4+ lesion indicated that 100 % of the glomerulus was involved. Thus, the mesangiolysis score (MES) was then obtained by multiplying the degree of damage (0 to 4+) by the percentage of the glomeruli with the lesion. Tubular injuries including tubular necrosis or occlusion of collecting ducts by cast material were graded as mild (1+), moderate (2+), or severe (3+).

Western Blot Analysis

Nuclear protein from whole kidney was prepared using NE-PER Nuclear and Cytoplasmic Extraction Reagents (Pierce Biotechnology, Inc. Rockford, Illinois, USA). Nuclear protein was electrophoresed using 10% SDS-PAGE gels and transferred to polyvinylidene difluoride membrane (Immobilon-P, Millipore Co., Bedford, Massachusetts, USA). A monoclonal IgG HIF-1α antibody α67 (Novus Biological, Littleton, Colorado, USA) was used; a horseradish peroxidase-conjugated antibody (Promega Co., Madison, USA) was used as a secondary antibody. The ECL Western blotting systems (Amersham Bioscience, Upsala, Sweden) was used for detection.

Immunohistochemical Analysis

Paraffin sections including the samples were dewaxed in xylene and rehydrated in a series of ethanol, and then washed in distilled water before staining procedures. According to the instruction provided by the manufacturer, HIF-1α was identified with rabbit polyclonal anti-HIF-1α antibody H-206 (Santa Cruz Biotechnology, California, USA) utilizing the catalyzed signal amplification system (Dako, Hamburg, Germany) based on the streptavidin-biotin-peroxidase reaction. Antigen retrieval was performed for 5 min in a preheated Dako target retrieval solution using a microwave. Incubation procedures were performed in a humidified chamber. Following the incubation, specimens were washed 3 times in TBST buffer. The specificity of staining was confirmed by substitution of the primary antibody for a normal rabbit IgG and additionally by an immunohistochemical reaction without a primary antibody but with the secondary antibody alone.

An Experiment using Cobalt Chloride as a Pretreatment

Rats were twice subcutaneously administered 30mg/kg of cobalt chloride ($CoCl_2$) at a 12 hour interval ($CoCl_2$ group) (n=11), followed by unilateral

nephrectomy. Then, the rats were administered with HV and AII. As a comparison, rats were injected with 0.9% NaCl solution instead of $CoCl_2$, followed by the same protocol as the $CoCl_2$ group (n=11). After $CoCl_2$ administration, however, before injection of HV and AII, a kidney was excised as a sample to examine expression level of HIF-1α ($CoCl_2$ Pre). Likewise, 2 days after administration of HV and AII, a kidney was also excised ($CoCl_2$ Day2). To compare the expression level of HIF-1α by $CoCl_2$ before GN and the severity of pathology of GN, we investigated whether pre-induction of HIF-1α is involved in renal protection.

Statistical Analysis

Data are reported as mean ± SEM. A paired *t* test was used for paired samples and Student's *t* test was used to compare the 2 groups. One-way layout analysis of variance or repeated measures of analysis of variance were used to compare multiple groups. If the p value was significant, Scheffe's multiple comparison was performed. A p value < 0.05 were considered significant.

Results

AII combined with HV developed GN

Morphological studies using PAS and PAM staining revealed that there are no glomerular or tubular injuries in N group (fig. 2A), HV group (fig. 2B), A group (fig. 2C), however, GN was detected only in the H+A group (fig. 2E). Although renal tubular casts were observed, glomerular changes were scarcely observed on day 1 after AII and HV administration (figs. 2D, 3). GN was initially detected on day 2 (figs. 2E, 2F, 3), followed by further aggravation during the time course (data not shown). Renal tubular injury including tubular necrosis was not remarkable, and extensive cellular infiltration was not found in the interstitial regions (fig. 3). On the other hand, characteristic focal and segmental mesangiolysis, explained as capillary aneurysmal ballooning, was observed with dilatation of glomerulus (figs. 2E, 2F). The rate of occurrence of GN on day 2 was 44.9±2.6 %, and the MES score of the H+A group was 199±15 (fig. 3). On the other hand, in the HV group, less than 2 % had morphologic changes of mesangiolysis during 4 days, and the MES score was 10±5 (figs. 2B, 3). Moreover, in the A group, there were no morphologic changes during the time course (fig. 2C).

Changes in serum UN and Cr

Serum UN and Cr were 18.4±0.7, 0.31±0.01 mg/dl, respectively, on day 2 in the N group. In the H+A group, serum UN and Cr levels increased to 41.5±4.0, 0.57±0.05 mg/dl, respectively, on day 2; significantly higher than those in the N group (figs. 4A, 4B). In contrast, serum UN and Cr levels in the H+A group on day 1 (24.0±1.8 and 0.42±0.02 mg/dl, respectively) were similar to the level of the N group. There were no significant differences in serum UN and Cr level among the HV, A and N groups.

SBP response

SBP values of each group are shown in figure 4C. There were no significant differences in SBP after nephrectomy among the 4 groups. Administration of AII caused a significant increase of SBP on day 1 (186±4 mmHg) and persisted to day 2 (192±1 mmHg). SBP in the H+A group on day 2 (183±3 mmHg) was comparable to that in the A group. Administration of HV had no influence on SBP during the 2 days.

Expression Level of HIF-1α Protein

Western blot analysis revealed that the expression level of HIF-1α protein increased in the H+A and A groups (fig. 5A), compatible with the results of immunohistochemical analysis. Expressions of HIF-1α protein were observed in the A and H+A groups, but protein expression was not detected in the N and HV groups. These data suggest that HIF-1α was induced mainly by AII, and, at least in part, was related to the pathogenesis of GN or to the defense mechanism against the progression of GN.

Induction of HIF-1α in Glomeruli and Renal Tubules

Immunohistochemical study demonstrated positive nuclear staining of HIF-1α in glomeruli, renal tubules (figs. 2I, 2J), collecting ducts and epithelium of the papilla (data not shown) in the A and H+A groups. In contrast, no positive nuclear signals were detected in the N (fig. 2H) and HV (data not shown) groups. HIF-1α positive cells were mainly detected in mesangial cells in glomeruli (figs. 2I, 2J). As demonstrated, especially in the H+A group (fig. 2J), HIF-1α was expressed in the intact part of the glomerulus, but not in the injured part of the same glomerulus. Furthermore, nuclear HIF-1α positive signals were observed in smooth muscle cells in peripheral renal arteries (data not shown).

$CoCl_2$ Pretreatment Inhibits the Progression of GN

To further investigate whether HIF-1α is involved in the development of nephropathy or in the anti-progressive action, we pretreated rats with $CoCl_2$. As demonstrated in fig. 5B, pretreatment with $CoCl_2$ increased HIF-1α expression before administration of HV and AII (Pre-1), suggesting that HIF-1α was induced by $CoCl_2$ before development of GN. Even on day 2, the expression level of HIF-1α was increased in the $CoCl_2$ group ($CoCl_2$ Day2-1). In the $CoCl_2$ group, focal mesangiolysis with glomeruli enlargement was still observed, but the number of GN was much less than in those without $CoCl_2$ pretreatment (fig. 2G).

Thus, 7 of 11 rats (63.6%) with $CoCl_2$ pretreatment were rescued from GN alone, while the other 4 (36.4%) were not; showing a comparable severity level of GN with the non-$CoCl_2$ group. As

demonstrated in fig. 5B, unlike Pre-1, Pre-2 did not induce HIF-1α with $CoCl_2$ and showed no $CoCl_2$ suppression of GN. The ratio between rats rescued or not-rescued from GN was comparable with that between pre-induction and non-induction of HIF-1α by $CoCl_2$, as demonstrated in fig. 5C. In the $CoCl_2$ group the rate of GN from each rat decreased to 12.2±2.1%, which was in great contrast to 44.9±2.6% in the non-$CoCl_2$ group. Furthermore, serum UN and Cr levels on day 2 were significantly lower in the $CoCl_2$ than in the non-$CoCl_2$ group ($p<0.05$) (figs. 6A, 6B), despite comparable SBP values between the 2 groups (fig. 6C).

Discussion

In this study, we developed a new model of GN induced by both HV and AII. This model has several distinct characteristics. First, GN developed rapidly, and was detected on the second day after administration of HV and AII. Many models of GN have been reported including 5/6 nephrectomized and Thy-1.1 nephritis models [18,19]. However, these models take a long time to develop nephropathy. In contrast, our protocol induced GN in 2 days, suggesting that one of the advantages our model has over others is in terms of the time course. Further, pathological findings were restricted to glomerular regions without remarkable tubular or interstitial lesions. Since our GN model developed within 2 days, our model also has advantages for disclosing the specifically critical time point of the development of GN. Further, the development rate of GN was almost 100%, indicating the high reproducibility of our model. This basis of the rat model was initially developed by Barnes JL et al. who reported that the progression of AII-induced renal injury was accelerated by preexisting injury induced by HV [20]; ours, which now optimizes the reproducibility of GN, is a modification of their model.

Habu induced nephropathy was reported to develop within 1 day by a dose of 2.0-4.0 mg/kg HV (in our model 3.5 mg/kg) and the main pathological change was "mesangiolysis" [21,22]. However, for reasons we haven't as yet ascertained, in our study no rats showed Habu-nephropathy specific pathological findings during the first week in the HV group. On the other hand, AII is one of the major factors responsible for the pathogenesis of GN, because it remarkably increases glomerular pressure causing hyperfiltration, production of extracellular matrix and expression of lines of genes involving GN [23-25]. Further, since AII has some ischemic effects on kidney, there is the possibility that an AII-induced ischemic effect causes the GN depicted in our model. However, as demonstrated in this study, glomerular injury was predominantly observed, and was not associated with renal tubular lesions, i.e., tubular necrosis suggesting renal ischemia. Therefore, in accordance with the pathological characteristic of this GN, AII-induced renal ischemia may not be responsible for the development in our model. Additionally, in this study, SBP increased in the A and A+H groups, but GN was not induced in the A group. Therefore, GN in our model was induced not by HV or AII alone, but by the combination of HV and AII, independent of any increase in systemic blood pressure.

HIF-1α is a master transcriptional factor, transactivating the expression of many genes important for cell survival under hypoxic conditions [11-13,26]. These genes are responsible for glycolysis, angiogenesis, proliferation and iron metabolism, all of which are induced by hypoxic stress; thus, the induction of HIF-1α is a marker of hypoxia. HIF-1α is regulated at the post-translational level by the proteasome system through ubiquitination with von Hippel Lindeau (VHL) protein [27,28]. As previously reported, this regulation of HIF-1α protein level is dependent on the concentration of oxygen. Hypoxia induces enhancement of HIF-1α protein stability leading to the elevation of the protein level due to inhibition of degradation by VHL. Therefore, hypoxia induces adaptation in cells including induction of HIF-1α; the hypoxic pathway. On the other hand, a line of evidence has recently accumulated that suggests that HIF-1α is also regulated independent of oxygen concentration through the non-hypoxic pathway [14,15]. AII is reported to regulate HIF-1α both at transcriptional and post-translational levels in vascular smooth muscle cells cultured under normoxic condition through the AII type 1 receptor [14,15]. Moreover, HIF-1α is also post-translationally regulated in several cell lines in the presence of tumor necrosis factor-α or nitric oxide independent of oxygen contents [29,30].

As demonstrated in this study, immunoreactivity of HIF-1α was not detected in the N group (no treatment group), but HIF-1α was detected in the nuclei of glomerular, tubular and epithelium cells of the papilla by administration of AII alone or AII and HV together. This is the first evidence showing that HIF-1α was detected in the kidney by AII, independent of systemic hypoxic stress. As indicated here, HIF-1α was found to be expressed only in intact, not damaged glomeruli. Even within a glomerulus, only the intact part of glomerular cells expressed HIF-1α. Considering the fact that induction of HIF-1α is one of the defense mechanisms for cell survival [31-33], our data indicate that induction of HIF-1α is a marker of glomeruli survival; indeed, it could be a marker of renal protection.

To further investigate whether HIF-1α is involved in the progression or protection of GN, pre-induction of HIF-1α was performed with $CoCl_2$ before administration of HV and AII. Surprisingly, the induction of HIF-1α by $CoCl_2$ pretreatment

attenuated the progression of GN; the level of GN was reduced from 44.9% to 12.2% and the incidence of GN was reduced from 100% to 36.4%. Furthermore, as indicated, the pre-induction of HIF-1α actually affects the inhibition of GN, because the rate of HIF-1α induction was parallel with that of the attenuation of GN. Therefore, our data suggest that HIF-1α is involved, at least in part, in the defense mechanism against the progression of GN, and hence could be a marker for renal protection.

AII is reported to induce HIF-1α [14,15] and it plays a partial role in the renal protective effect; however, the other effects of AII, such as increasing glomerular pressure and modulating gene expression involving in the renal failure, may overcome any protective effect of AII-induced HIF-1α, and so as a result it may lead to the progression of GN.

In conclusion, we developed a highly reproducible GN model by combining HV and AII. Pre-induction of HIF-1α remarkably attenuated the progression of GN, indicating that HIF-1α was involved in the defense mechanism of the kidney.

Acknowledgments

This work was supported by Grants-in-Aid for Scientific Research from the Ministry of Education, Science and Culture (#14657409). We thank Dr. Masami Nakatani, Dr. Noriko Kishimoto, Dr. Ichiro Yamasaki, Dr. Yoshitaka Kumon, Dr. Hiroaki Takeuchi, Dr. Jun Imamura, Dr. Mikio Kamioka, Ms. Chiaki Kawada, Ms. Chizuko Sugimoto, and Mr. Takuya Yamaguchi for their helpful advice, and generous support.

References

1 Rifai A, Small PA Jr, Teague PO, Ayoub EM: Experimental IgA nephropathy. J Exp Med 1979; 150: 1161-1173.
2 Ishizaki M, Masuda Y, Fukuda Y, Yamanaka N, Masugi Y, Shichinohe K, Nakama K: Renal lesions in a strain of spontaneously diabetic WBN/Kob rats. Acta Diabetol Lat 1987; 24: 27-35.
3 Banks KL: Glomerulonephritis, autoimmunity, autoantibody. Animal model: anti-glomerular basement membrane antibody in horses. Am J Pathol 1979; 94: 443-446.
4 Elzinga LW, Rosen S, Bennett WM: Dissociation of glomerular filtration rate from tubulointerstitial fibrosis in experimental chronic cyclosporine nephropathy: role of sodium intake. J Am Soc Nephrol 1993; 4: 214-221.
5 Arendshorst WJ, Finn WF, Gottschalk CW: Pathogenesis of acute renal failure following temporary renal ischemia in the rat. Circ Res 1975; 37: 558-568.
6 Wilson CB, Dixon FJ: Immunopathologic mechanisms of renal disease. Ric Clin Lab 1975; 5: 17-38.
7 Masuda Y, Shimizu A, Mori T, Ishiwata T, Kitamura H, Ohashi R, Ishizaki M, Asano G, Sugisaki Y, Yamanaka N: Vascular endothelial growth factor enhances glomerular capillary repair and accelerates resolution of experimentally induced glomerulonephritis. Am J Pathol 2001; 159: 599-608.
8 Kim S, Iwao H: Molecular and cellular mechanisms of angiotensin II-mediated cardiovascular and renal diseases. Pharmacol Rev 2000; 52: 11-34.
9 Lee LK, Meyer TW, Pollock AS, Lovett DH: Endothelial cell injury initiates glomerular sclerosis in the rat remnant kidney. J Clin Invest 1995; 96: 953-964.
10 Huang LE, Arany Z, Livingston DM, Bunn HF: Activation of hypoxia-inducible transcription factor depends primarily upon redox-sensitive stabilization of its alpha subunit. J Biol Chem 1996; 271: 32253-32259.
11 Wang, GL, Jiang BH, Rue EA, and Semenza GL: Hypoxia-inducible factor 1 is a basic-helix-loop-helix-PAS heterodimer regulated by cellular O2 tension. Proc Natl Acad Sci USA 1995; 92: 5510-5514,
12 Rosenberger C, Mandriota S, Jurgensen JS, Wiesener MS, Horstrup JH, Frei U, Ratcliffe PJ, Maxwell PH, Bachmann S, Eckardt KU: Expression of hypoxia-inducible factor-1alpha and -2alpha in hypoxic and ischemic rat kidneys. J Am Soc Nephrol 2002; 13: 1721-1732.
13 Wenger RH, Rolfs A, Marti HH, Guenet JL, and Gassmann M: Nucleotide sequence, chromosomal assignment and mRNA expression of mouse hypoxia-inducible factor-1 alpha. Biochem Biophys Res Commun 1996; 223: 54-59,
14 Richard DE, Berra E, Pouyssegur J: Nonhypoxic pathway mediates the induction of hypoxia-inducible factor 1alpha in vascular smooth muscle cells. J Biol Chem 2000; 275: 26765-26771.
15 Page EL, Robitaille GA, Pouyssegur J, Richard DE: Induction of hypoxia-inducible factor-1alpha by transcriptional and translational mechanisms. J Biol Chem 2002; 277: 48403-48409.
16 Raij L, Azar S, Keane W: Mesangial immune injury, hypertension, and progressive glomerular damage in Dahl rats. Kidney Int 1984; 26: 137-143.
17 Linas SL, Shanley PF, Whittenburg D, Berger E, Repine JE: Neutrophils accentuate ischemia-reperfusion injury in isolated perfused rat kidneys. Am J Physiol 1988; 255: F728-F735.
18 Romero F, Rodriguez-Iturbe B, Parra G, Gonzalez L, Herrera-Acosta J, Tapia E: Mycophenolate mofetil prevents the progressive renal failure induced by 5/6 renal ablation in rats. Kidney Int 1999; 55: 945-955.
19 Kaneko Y, Shiozawa S, Hora K, Nakazawa K: Glomerulosclerosis develops in Thy-1 nephritis under persistent accumulation of macrophages. Pathol Int 2003; 53: 507-517.
20 Barnes JL, Lisa MS: Origin of interstitial fibroblasts in an accelerated model of angiotensin II (AII)-induced interstitial fibrosis. J Am Soc Nephrol 2001; 12: 699A3645.
21 Cattell V, Bradfield JW: Focal mesangial proliferative glomerulonephritis in the rat caused by habu snake venom. A morphologic study. Am J Pathol 1977; 87: 511-524.
22 Kitamura H, Sugisaki Y, Yamanaka N: Endothelial regeneration during the repair process following Habu-snake venom induced glomerular injury. Virchows Arch. 1995; 427: 195-204.
23 Ruggenenti P: Angiotensin-converting enzyme inhibition and angiotensin II antagonism in nondiabetic chronic nephropathies. Semin Nephrol 2004; 24: 158-167.

24 Tolins JP, Raij L: Effects of amino acid infusion on renal hemodynamics. Role of endothelium-derived relaxing factor. Hypertension 1991; 17: 1045-1051.
25 Nakamura T, Obata J, Kimura H, Ohno S, Yoshida Y, Kawachi H, Shimizu F: Blocking angiotensin II ameliorates proteinuria and glomerular lesions in progressive mesangioproliferative glomerulonephritis. Kidney Int 1999; 55: 877-889.
26 Makino Y, Cao R, Svensson K, Bertilsson G, Asman M, Tanaka H, Cao Y, Berkenstam A, Poellinger L: Inhibitory PAS domain protein is a negative regulator of hypoxia-inducible gene expression. Nature 2001; 414: 550-554.
27 Neckers LM: aHIF: the missing link between HIF-1 and VHL? J Natl Cancer Inst 1999; 91: 106-107.
28 Maxwell PH, Wiesener MS, Chang GW, Clifford SC, Vaux EC, Cockman ME, Wykoff CC, Pugh CW, Maher ER, Ratcliffe PJ: The tumour suppressor protein VHL targets hypoxia-inducible factors for oxygen-dependent proteolysis. Nature 1999; 399: 271-275.
29 Zhou J, Fandrey J, Schumann J, Tiegs G, Brune B: NO and TNF-alpha released from activated macrophages stabilize HIF-1alpha in resting tubular LLC-PK1 cells. Am J Physiol Cell Physiol 2003; 284: C439-C446.
30 Sandau KB, Zhou J, Kietzmann T, Brune B: Regulation of the hypoxia-inducible factor 1alpha by the inflammatory mediators nitric oxide and tumor necrosis factor-alpha in contrast to desferroxamine and phenylarsine oxide. J Biol Chem 2001; 276: 39805-39811.
31 Prass K, Ruscher K, Karsch M, Isaev N, Megow D, Priller J, Scharff A, Dirnagl U, Meisel A: Desferrioxamine induces delayed tolerance against cerebral ischemia in vivo and in vitro. J Cereb Blood Flow Metab 2002; 22: 520-525.
32 Furuta GT, Turner JR, Taylor CT, Hershberg RM, Comerford K, Narravula S, Podolsky DK, Colgan SP: Hypoxia-inducible factor 1-dependent induction of intestinal trefoil factor protects barrier function during hypoxia. J Exp Med 2001; 193: 1027-1034.
33 Matsumoto M, Makino Y, Tanaka T, Tanaka H, Ishizaka N, Noiri E, Fujita T, Nangaku M: Induction of renoprotective gene expression by cobalt ameliorates ischemic injury of the kidney in rats. J Am Soc Nephrol 2003; 14: 1825-1832.

Figure Legends

Fig. 1. Study Protocol. All rats are unilaterally nephrectomized on day -1 and divided into 4 groups on day 0.
N group; no injection of reagents. HV group; injection of 3.5mg/kg of Habu snake venom (HV). A group; continuous administration of 100ng/min of Angiotensin II (AII). H+A group; administration of HV and AII.

Fig. 2. Glomerulonephritis is developed with the combination of HV and AII, and HIF-1α is induced in the intact glomeruli.
There are no glomerular or tubular injuries in N group (**A**), HV group (**B**), A group (**C**) and H+A group on day 1 (**D**). Damaged glomeruli, characterized by extensive mesangiolysis, are observed in H+A group on day 2. PAS staining. Magnification, *100 (**E**). Focal and segmental mesangiolysis with large capillary aneurysmal ballooning are observed in the H+A group on day 2. PAM staining. Magnification, *400 (**F**). The number of GN was significantly less in pre-treatment with $CoCl_2$ than without. PAS staining. Magnification, *100 (**G**). Immunoreactive HIF-1α positive signals are not detected in the N group (**H**). Nuclear HIF-1α signals are observed in a glomerulus and tubules in the A group. Magnification, *200 (**I**). A glomerulus in the H+A group on day 2 possesses intact cells with HIF-1α positive signals, in contrast, other parts have few HIF-1α signals due to mesangiolysis. Magnification, *200 (**J**).

Fig. 3. Semiquantitative analysis of morphologic changes in our glomerulonephritis model. The main lesion in the H+A group is initially detected on day 2 as mesangiolysis in glomeruli; however, there are no tubular lesions of necrosis except for tubular casts; in contrast, there are no morphological changes in the N and A groups. MES, Mesangiolysis score.

Fig. 4. Serum UN, Cr and SBP are increased with the combination of HV and AII. The serum UN (**A**) and Cr (**B**) levels in the H+A group on day 2 are significantly higher than other groups. SBP increases significantly with administration of AII (A and H+A groups) (**C**).

Fig. 5. The protein level of HIF-1α is increased by administration of HV and AII, and pretreatment of $CoCl_2$ increases HIF-1α expression before development of GN. HIF-1α is not detected in the N and HV groups (Day2). However, HIF-1α is detected in A (Day2) and H+A (Days 1 and 2) groups (A). The $CoCl_2$ group, in accord with the level of HIF-1α induction, was divided into two groups. HIF-1α is greatly induced before the development of GN ($CoCl_2$ group Pre-1), and is followed by a high level ($CoCl_2$ group Day2-1); in contrast, it is not efficiently induced ($CoCl_2$ group Pre-2), and also is scarcely detected on day 2 ($CoCl_2$ group Day2-2) (B). The rate of pre-induction of HIF-1α by $CoCl_2$ is comparable with that of the inhibition of GN by $CoCl_2$ (C).

Fig. 6. Pretreatment with $CoCl_2$ attenuates GN. Serum UN (A) and Cr (B) levels in the $CoCl_2$ group on day 2 are significantly decreased compared to those in the non-$CoCl_2$ group. There is no significant difference in SBP between the $CoCl_2$ and non-$CoCl_2$ groups (C).

Fig. 1

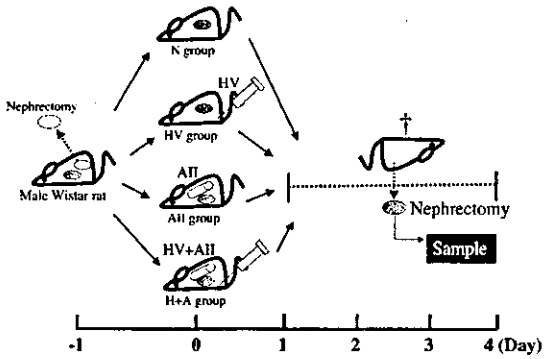

Fig. 2

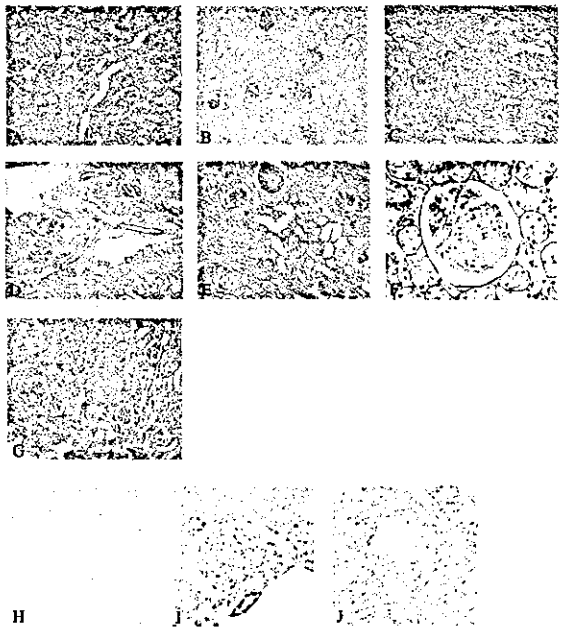

Fig. 3

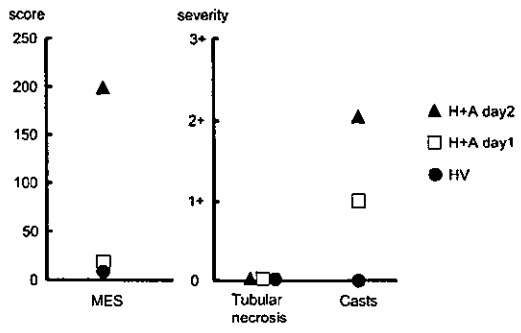

Fig. 3

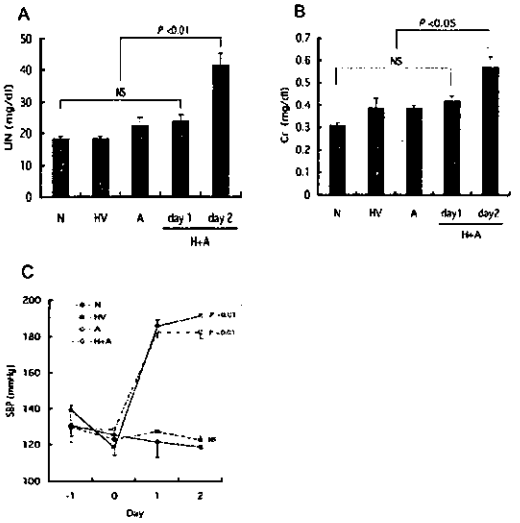

Fig. 4

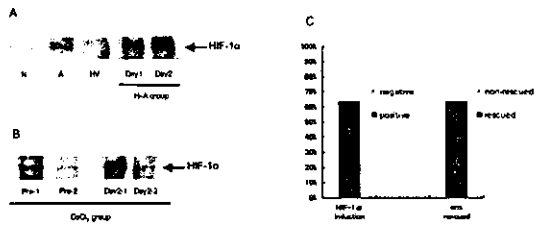

Fig. 5

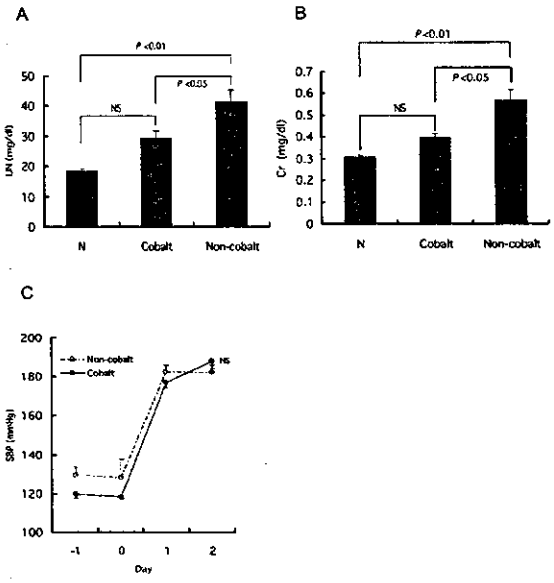

Effect of Electrical Modification of Cardiomyocytes on Transcriptional Activity through 5′-AMP-activated Protein Kinase

Yoshihiko Kakinuma, Yanan Zhang†, Motonori Ando*, Tetsuro Sugiura†, and Takayuki Sato**

Abstract: Endothelin-1 (ET-1) is known as an aggravating factor of the failing cardiomyocytes and, therefore, a therapeutic method is indispensable to decrease cardiac ET-1 expression. To study the mechanisms of how cardiac ET-1 gene expression can be modified, we investigated the effect of electrical stimulation against cardiomyocytes. Considering the physiology of cardiomyocytes, in vitro cultured cardiomyocytes demonstrate distinctive features from in vivo cardiomyocytes (i.e. the absence of a stretch along with electrical stimulation). In this study, we especially focused on the effect of electrical stimulation. The electrical stimulation reduced the gene expression of ET-1 mRNA in rat primary cultured cardiomyocytes. Furthermore, this effect on the transcriptional modification of ET-1 was also identified in H9c2 cells. Luciferase activity using H9c2 cells was decreased by electrical stimulation in the early phase, suggesting that the attenuation of the ET-1 gene transcription by electrical stimulation should be due to a transcriptional repression. To further investigate a trigger signal involved in the transcriptional repression, phosphorylation of 5′-AMP-activated protein kinase (AMPK) was evaluated. It was revealed that AMPK was phosphorylated in the early phase of electrical stimulation of H9c2 cells as well as in rat primary cultured cardiomyocytes, and that AMPK phosphorylation was followed by ET-1 transcriptional repression, suggesting that electrical stimulation directly regulates AMPK. This study suggests that AMPK activation in cardiomyocytes plays a crucial role in the transcriptional repression of ET-1.

Key Words: endothelin-1, cardiomyocytes, 5′-AMP-activated protein kinase

(*J Cardiovasc Pharmacol*™ 2004;44(suppl 1):S435–S438)

The endothelin (ET) system is known to be indispensable for the development of the heart. In the developmental stage, ET-1 exerts the formation of the heart through the receptors endothelin-A and endothelin-B, and the system exerts the biological function through either autocrine or paracrine fashion. It has been reported that deformity of the heart is produced in the absence of the ET system. Especially, cardiomyocytes have been reported to remarkably express and produce ET-1 in the pathophysiological condition (i.e. the failing heart) compared with the normal heart.[1] The mechanisms have been extensively studied of how the failing heart expresses ET-1 in the progression of heart failure; however, our previous study clearly demonstrated one aspect of the mechanisms — impaired cardiac energy metabolism.[2] The level of cardiac ET-1 gene expression is dependent on the condition of the cardiomyocytes in vivo; the failing cardiomyocytes produce more ET-1. However, even normal primary cultured cardiomyocytes in vitro could extraordinarily express ET-1 compared with in vivo. The abnormal pattern of cardiac ET-1 gene expression in vitro is also accompanied with a surprising switch of the myosin heavy chain isoform from α to β (a fetal pattern), suggesting that our cultured cardiomyocytes have already biologically changed their character.[3] However, this finding might provide us with some therapeutic clue as to how cardiac ET-1 expression can be depressed using cultured cardiomyocytes. If we could obtain some tool to repress cardiac ET-1 gene expression in vitro, it might lead to clarification of one of the therapeutic strategies against heart failure. Consequently we have so far concentrated on searching for ways to decrease cardiac ET-1 gene expression. Among them, we have found several methods to modify the expression using not chemicals or drugs, but physical stimulation.[3] In this study, using electrical stimulation (ES) we have successfully inhibited the cardiac ET-1 gene expression, and investigated the mechanisms by which such stimulation causes a depression of the gene expression.

METHODS

Cell Culture of Rat Cardiomyocytes and H9c2 Cells

According to our previous studies,[1] cardiomyocytes were isolated from 2-day-old Wistar–Kyoto rats. 5-Amino-imidazole-4-carboxamide-1-β-D-ribofuranosyl 5-monophosphate (AICAR) was purchased from Sigma (St Louis, MO, U.S.A.), and H9c2 cells were transiently treated by AICAR.

*Department of Cardiovascular Control and †Department of Laboratory Medicine, Kochi Medical School, Nankoku, Kochi, Japan
Address correspondence and reprint requests to Yoshihiko Kakinuma, Department of Cardiovascular Control, Kochi Medical School, Kohasu, Nankoku-shi, Kochi-ken 783-8505, Japan. E-mail: kakinuma@med.kochi-u.ac.jp
This study was supported by a Health and Labor Sciences Research Grant (H14-NANO-002) for Advanced Medical Technology from the Ministry of Health, Labor, and Welfare of Japan.

Electrical Stimulation

We have developed a specific ES device, which is modified to simultaneously provide multi-channels of ES and also to efficiently regulate bidirectional current. Our protocol for ES was performed as follows: 10 V, 10 milliseconds of duration and 4 Hz of frequency.

RNA Isolation and Reverse Transcription-Polymerase Chain Reaction

As previously described, total RNA was isolated, and 1 μg total RNA was reverse-transcribed and used for a polymerase chain reaction (PCR) template. PCR primers were prepared for preproET-1, hypoxia-inducible factor (HIF)-1α, β-actin,[2,3] and glucose transporter 3.

Luciferase Assay

As previously reported, the 5′-regulatory region of preproET-1 gene was subcloned into a luciferase vector.[2] The reporter vector was transfected into H9c2 cells by a cationic reagent, Effecten (QIAGEN, Valencia, CA, U.S.A.), according to the manufacture's protocol. Forty-eight hours after transfection, cells were lysed for evaluation of luciferase activity.

Western Blot Analysis

Cells were harvested from dishes by scraping, were washed with phosphate-buffered saline, and cell lysates were mixed with sample buffer. The samples were fractionated by sodium dodecyl sulfate-polyacrylamide gel electrophoresis and transferred onto membranes (Millipore Corp., Bedford, MA, U.S.A.). After transfer into the membrane, they were soaked in blocking buffer. The membranes were incubated with a monoclonal phosphor-5′-AMP-activated protein kinase-α (Thr172) antibody (1:1000; Cell Signaling Technology, Beverly, MA, U.S.A.). After the membranes were washed, horseradish peroxidase-conjugated secondary antibodies (Promega, Madison, WI, U.S.A.) were applied and the signal was detected using an enhanced chemi-luminescence system (Amersham, Piscataway, NJ, U.S.A.).

RESULTS

Electrical Stimulation Affects Gene Expression of Rat Cardiomyocytes

To investigate transcriptional regulation of cardiomyocytes, primary cultured cardiomyocytes were subjected to ES. Even with a bi-directional current, cardiomyocytes could not be cultured for ES more than 16 hours. As demonstrated in Fig. 1, ES remarkably decreased gene expression of preproET-1 and HIF-1α in the cardiomyocytes, compared with non-stimulated cardiomyocytes. However, the mRNA level of β-actin was not decreased by ES. Adversely, gene expression of glucose transporter 3 mRNA was increased by ES. These results suggested that

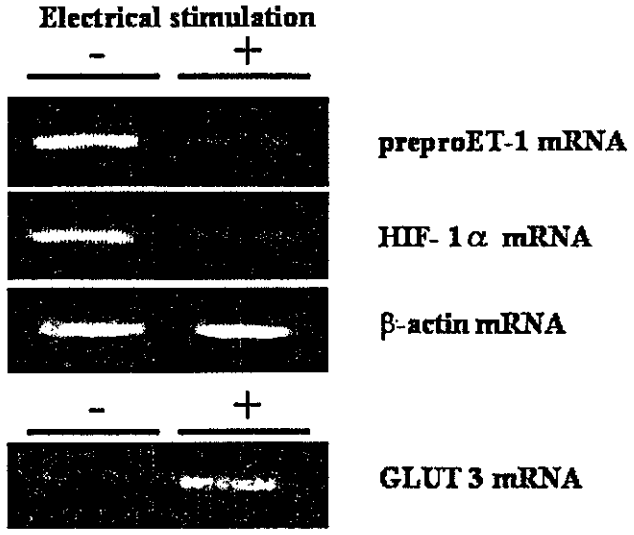

FIGURE 1. Electrical stimulation (ES) modifies gene expression of preproendothelin-1 (preproET-1), hypoxia-inducible factor-1α (HIF-1α), and glucose transporter (GLUT) 3 mRNAs. PreproET-1 and HIF-1α gene expressions were decreased 5 hours after ES. In contrast, GLUT 3 gene expression was increased by ES. The level of β-actin mRNA was not affected by ES.

cardiomyocytes respond to ES with an increased gene expression of glucose transporter 3; however, in contrast, such an ES modified gene expression of cardiac preproET-1 and HIF-1α.

Electrical Stimulation Transcriptionally Regulates PreproET-1 Gene Expression

Further to investigate especially the gene expression of preproET-1 mRNA, a reporter assay was performed using a reporter vector possessing the 5′-promoter regulatory region of the preproET-1 gene. H9c2 cells, a cell line of rat ventricular cardiomyocytes, were transfected by the reporter vector. As shown in Fig. 2, ES of H9c2 cells greatly decreased the luciferase activity of preproET-1. The phenomenon of the depressed luciferase activity was compatible with the decreased preproET-1 mRNA by reverse transcription-PCR.

Electrical Stimulation Elevates Phosphorylation of 5′-AMP-activated Protein Kinase

To investigate mechanisms to decrease a transcriptional level of preproET-1, we studied whether ES activates the phosphorylation of 5′-AMP-activated protein kinase (AMPK) using H9c2 cells. The time course study demonstrated that AMPK phosphorylation was detected soon after ES (Fig. 3). Furthermore, such an increase in AMPK phosphorylation was also observed in primary cultured cardiomyocytes. It was suggested that ES causes activation of

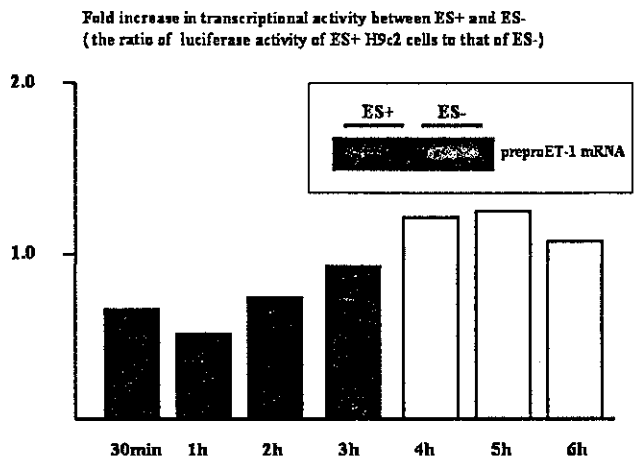

FIGURE 2. Electrical stimulation (ES) transcriptionally represses preproendothelin-1 (preproET-1) gene expression in H9c2 cells. Gene expression of preproET-1 in H9c2 cells was also decreased by ES. Using a reporter vector of the preproET-1 gene, luciferase activity was compared between electrical stimulated (ES+) H9c2 cells and non-electrical stimulated (ES–) cells. The ratio of luciferase activity of ES+ to that of ES– was measured, where a ratio > 1 suggests transcriptional activation, contrasting with a ratio < 1 suggesting repression.

AMPK with a comparable time course of suppression of the preproET-1 gene, and consequently that AMPK phosphorylation is profoundly related to the repression of transcriptional activity of preproET-1 gene expression.

An Activator of AMPK Causes a Decrease in PreproET-1 mRNA

H9c2 cells were treated by AICAR, which is known as an activator of AMPK. As demonstrated in Fig. 3, AICAR increased the phosphorylation of AMPK. The activation of AMPK occurred very rapidly with a comparable time course of ES. With treatment of AICAR, the mRNA level of preproET-1 was decreased (Fig. 4). It was suggested that AMPK activation was involved in the attenuated preproET-1mRNA gene expression.

DISCUSSION

ET-1 is one of the aggravating factors in heart failure, because ET-1 further activates the glycolytic system in the failing cardiomyocytes, resulting in aggravation of malfunction in the heart. Therefore, one of the therapeutic goals that inhibit the progression of heart failure might be to decrease cardiac ET-1 gene expression. There are many manipulations to decrease ET-1 gene expression, including blocking the renin–angiotensin system and ET receptor antagonists.[4] However, we have further investigated whether other manipulations can modify the cardiac ET-1 expression,

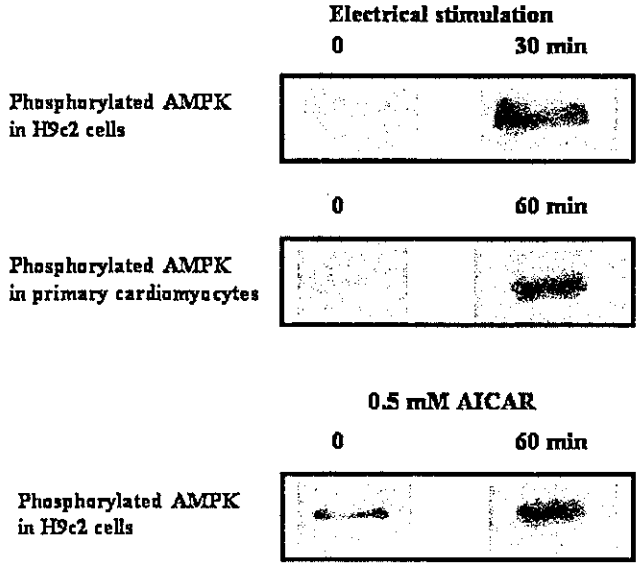

FIGURE 3. 5′-AMP-activated protein kinase (AMPK) is activated through phosphorylation by electrical stimulation (ES). ES caused activation of AMPK through phosphorylation in H9c2 cells. This phenomenon was also detected in rat primary cultured cardiomyocytes with a comparable time course. Also, 0.5 m*M* 5-aminoimidazole-4-carboxamide-1-β-D-ribofuranosyl 5-monophosphate (AICAR), an activator of AMPK, phosphorylated AMPK.

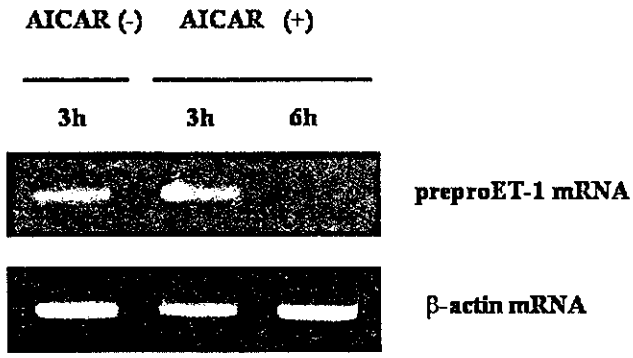

FIGURE 4. 5′-AMP-activated protein kinase activator decreases preproendothelin-1 (preproET-1) gene expression in H9c2 cells. 5-Aminoimidazole-4-carboxamide-1-β-D-ribofuranosyl 5-monophosphate (AICAR) 1.5 m*M* treatment remarkably decreased the gene expression of preproET-1 mRNA in H9c2 cells.

and then finally we have identified that a mechanical stimulation (i.e. ES) decreases cardiac ET-1 expression through activation of AMPK.

AMPK is known as a fuel sensor kinase, which is activated through phosphorylation when a cellular adenosine triphosphate (ATP) level is decreased.[5] Consequently, cells respond to a shortage of the energy and activate the

phosphorylation of AMPK. This kinase is therefore activated in the early phase to stimuli that might cause mitochondrial dysfunction, leading to ATP deprivation. This response through AMPK phosphorylation is considered an adaptation of cells to avoid cellular death with a shortage of ATP. However, this response is not only involved in pathological states, but also in physiological states. For example, exercise-induced muscle hypertrophy leads to remarkable adaptation of the muscle to the more efficient utilization of energy (i.e. mitochondrial β-oxidation of fatty acid), and consequently to activation of the mitochondrial function.[6] In the case of exercise, AMPK in skeletal muscle is known to be activated.[7] Therefore, it is suggested that the activation of AMPK through phosphorylation is followed by enhancement of mitochondrial function in a physiological condition to obtain more adequate ATP.

It is known that the cardiomyocytes obtain ATP predominantly through mitochondrial β-oxidation of fatty acid; however, when cardiomyocytes were treated by hypoxia, the cardiac energy metabolic system was changed from β-oxidation to glycolysis, because fatty acid oxidation is impaired. In such a case, as our previous study demonstrated, HIF-1α is induced for upregulation of glycolytic enzymes, and furthermore HIF-1α transcriptionally activates preproET-1 gene expression in the failing heart.[2] It is suggested that cardiac ET-1 expression is accompanied with a cellular glycolysis-dominant energy system.[8] With these findings in mind, further speculation is as follows: if the glycolysis-dominant energy system is inhibited, and alternatively mitochondrial β-oxidation of fatty acid is activated, ET-1 gene expression could be decreased. As our present study demonstrated, ES activates the phosphorylation of AMPK in a rapid fashion, followed by a decrease in the transcriptional activity of ET-1.

This is a first demonstration of transcriptional repression of cardiac preproET-1 gene expression using methods other than drugs. Moreover, this reaction is very rapid to decrease preproET-1 mRNA. Therefore, it is suggested that the manipulation of cardiomyocytes by ES is one candidate method to inhibit an increase in cardiac ET-1 gene expression.

REFERENCES

1. Kakinuma Y, Miyauchi T, Kobayashi T, et al. Myocardial expression of endothelin-2 is altered reciprocally to that of endothelin-1 during ischemia of cardiomyocytes *in vitro* and during heart failure *in vivo*. *Life Sci.* 1999;65:1671–1683.
2. Kakinuma Y, Miyauchi T, Yuki K, et al. Novel molecular mechanism of increased myocardial endothelin-1 expression in the failing heart involving the transcriptional factor hypoxia inducible factor-1α induced for impaired myocardial energy metabolism. *Circulation.* 2001;103: 2387–2394.
3. Kakinuma Y, Miyauchi T, Suzuki T, et al. Enhancement of glycolysis in cardiomyocytes elevates endothelin-1 expression through the transcriptional factor HIF-1α. *Clin Sci.* 2002;103(suppl. 48):210S–214S.
4. Sakai S, Miyauchi T, Kobayashi T, et al. Inhibition of myocardial endothelin pathway improves lomg-term survival in heart failure. *Nature.* 1996;384:353–355.
5. Winder WW. Energy-sensing and signaling by AMP-activated protein kinase in skeletal muscle. *J Appl Physiol.* 2001;91:1017–1028.
6. Saha AK, Schwarsin AJ, Roduit R, et al. Activation of malonyl-CoA decarboxylase in rat skeletal muscle by contraction and the AMP-activated protein kinase activator 5-aminoimidazole-4-carboxamide-1-β-D-ribofuranoside. *J Biol Chem.* 2000;275:24279–24283.
7. Hood DA. Plasticity in skeletal, cardiac, and smooth muscle invited review: contractile activity-induced mitochondrial biogenesis in skeletal muscle. *J Appl Physiol.* 2001;90:1137–1157.
8. Wu-Wong JR, Berg CE, Kramer D. Endothelin stimulates glucose uptake via activation of endothelin-A receptor in neonatal rat cardiomyocytes. *J Cardiovasc Pharmacol.* 2000;36(5 suppl. 1): S179–S183.

IEICE TRANS. ELECTRON., VOL.E87–C, NO.6 JUNE 2004

PAPER Special Section on Analog Circuit and Device Technologies

A Small-Chip-Area Transceiver IC for Bluetooth Featuring a Digital Channel-Selection Filter

Masaru KOKUBO[†a)], Masaaki SHIDA[†], Takashi OSHIMA[†], Yoshiyuki SHIBAHARA[†], Tatsuji MATSUURA[††], Kazuhiko KAWAI[††], *Members*, Takefumi ENDO[††], Katsumi OSAKI[††], Hiroki SONODA[††], Katsumi YAMAMOTO[††], Masaharu MATSUOKA[††], Takao KOBAYASHI[††], Takaaki HEMMI[††], Junya KUDOH[††], Hirokazu MIYAGAWA[††], Hiroto UTSUNOMIYA[††], Yoshiyuki EZUMI[††], Kunio TAKAYASU[††], Jun SUZUKI[††], Shinya AIZAWA[††], Mikihiko MOTOKI[††], Yoshiyuki ABE[††], Takao KUROSAWA[††], *and* Satoru OOKAWARA[††], *Nonmembers*

SUMMARY We have proposed a new low-IF transceiver architecture to simultaneously achieve both a small chip area and good minimum input sensitivity. The distinctive point of the receiver architecture is that we replace the complicated high-order analog filter for channel selection with the combination of a simple low-order analog filter and a sharp digital band-pass filter. We also proposed a high-speed convergence AGC (automatic gain controller) and a demodulation block to realize the proposed digital architecture. For the transceiver, we further reduce the chip area by applying a new form of direct modulation for the VCO. Since conventional VCO direct modulation tends to suffer from variation of the modulation index with frequency, we have developed a new compensation technique that minimizes this variation, and designed the low-phase noise VCO with a new biasing method to achieve large PSRR (power-supply rejection ratio) for oscillation frequency. The test chip was fabricated in 0.35-μm BiCMOS. The chip size was $3 \times 3\,mm^2$; this very small area was realized by the advantages of the proposed transceiver architecture. The transceiver also achieved good minimum input sensitivity of -85 dBm and showed interference performance that satisfied the requirements of the Bluetooth standard.

key words: *Bluetooth transceiver, low-IF, VCO, channel-selection filter*

1. Introduction

Recently, lots of useful mobile communication devices have been reaching the consumer market, and the ability to use such devices almost anywhere is bringing big benefits to the many users. Furthermore, wireless transceivers that make direct inter-device wireless data communication possible are finally becoming popular, and will dramatically improve the versatility of mobile devices such as cellular phones, PDAs, and portable personal computers.

A new standard named Bluetooth is the best-known of the wireless interface standards. Bluetooth defines a method of communication that covers a 10-m range [1]. Therefore, many transceiver ICs that implement the Bluetooth wireless standard have been developed [2]–[13]. Since Bluetooth transceivers are being embedded in many kinds of consumer equipment, size and cost are important issues, so the required ICs must be cheap and have small chip areas. Furthermore, the minimum input sensitivity expected of the transceivers improves year by year.

All designs to date for such RF transceivers include an analog channel-selection filter. However, since both RF (radio frequency) and IF (intermediate frequency) analog components must be integrated on the chip, designing the latter to include a channel selection filter is very difficult in a chip with a reasonable area. In particular, since the channel selection filter's cut-off frequency range is very low and its noise level has to be low, its component values are large and the filter occupies a big chip area. We have thus proposed an all-digital receiver architecture for Bluetooth transceivers and demonstrated its advantage in terms of chip-area reduction [14].

The strict interference performance specifications of the Bluetooth standard require that the channel-selection filter be implemented as a particularly high-order band-pass filter; in fact, tenth to fourteenth-order filters are required. The quality (Q) factor of the filter should also be very high; furthermore, large-value capacitors must be integrated into the chip to reduce levels of circuit-generated noise. Therefore, it is very difficult to achieve both a small chip area and good minimum input sensitivity for the transceiver.

We have adopted a new digital receiver architecture to simultaneously achieve both a small chip and good minimum input sensitivity. The distinctive point of this architecture is that we replace the complicated high-order analog filter for channel selection with the combination of a simple low-order analog filter and a sharp digital band-pass filter. Furthermore, we employ a digital demodulator in the receiver to take further advantage of fine-design-rule semiconductor processes and improve the receiver's minimum input sensitivity.

We further reduce the chip area by applying a novel transmitter architecture, that is, a new form of direct modulation for the VCO. Since conventional VCO direct modulation tends to suffer from variation of the modulation index with frequency, we have developed a new compensation technique that minimizes this variation.

We have fabricated the new Bluetooth transceiver IC with 0.35-μm BiCMOS technology and evaluated its performance. In this paper, we describe the transceiver architecture and the design of its core components in Sect. 2, and give the results of evaluation of the fabricated transceiver in

Manuscript received October 21, 2003.
Manuscript revised January 15, 2004.

[†]The authors are with Hitachi Ltd., Kokubunji-shi, 185-8601 Japan.
[††]The authors are with Renesas Technologies Co., Takasaki-shi, 370-0021 Japan.
a) E-mail: m-kokubo@crl.hitachi.co.jp

Sect. 3.

2. Transceiver Block Diagram

A block diagram of the transceiver is given in Fig. 1. If we want a small chip, we need a simple transceiver architecture [15]. We thus adopt a low-IF (low-intermediate-frequency) receiver and a novel form of VCO direct modulation.

2.1 Receiver

The signal received at the antenna is transferred to the RF filter via an antenna switch (SW). The RF filter passes the frequency band component between 2.4 and 2.5 GHz, which is used for ISM (industrial, scientific, and medical) applications. The output of the RF filter is input to the low-noise amplifier (LNA), which amplifies the input signal to the desired signal level without severe noise degradation. The RF output of the LNA is converted to the desired intermediate frequency by the mixer (MIX), and is transferred into a band-pass filter for channel selection. Finally, the demodulator (DEMOD) demodulates the output of the band-pass filter to generate the received data (RX-DATA).

We adopted a low-IF receiver architecture. With this architecture, selection of an appropriate center frequency is very important. Two constraints affect the selection of IF frequency: the settling time of the band-pass filter and the interference-suppression ratio. Our results of simulation, shown in Fig. 2, indicate that if we want an IF frequency higher than 2 MHz, the band-pass-filter's settling time has to be less than 6 μs. The conditions of this simulation are (1) allowance for the frequency offset between the received and local reference signals and (2) eye degradation of no more than 2 dB. Furthermore, if a lower IF frequency is used for the receiver, we obtain a better interference-suppression ratio, therefore, we used 2-MHz IF frequency.

The low-IF architecture lets us implement an on-chip channel-selection filter. The problem is that a large Q factor, greater than three, is necessary to secure a sufficient level of loss for interference components in the channel filter. However, an analog filter with a large Q factor is unsatisfactory in this role, since an area-hungry large capacitor must be applied to avoid amplification of thermal noise generated by the resistors.

This is why we realize the channel-selection filter as a digital filter, only using an analog filter to keep the input signal within the dynamic range of the ADC. Furthermore, an AGC (automatic gain controller) capable of high-speed convergence is also very important for our proposed digital architecture, because of the frequency-hopping access method used by Bluetooth transceivers.

Detailed descriptions of the receiver blocks follow.

2.1.1 LNA and Mixer

The LNA is shown in Fig. 3. The RF signal is provided to the LNA through a matching network from the RF input node (V_{RF}). The LNA consists of two common-emitter cascaded amplifiers with symmetrical layout. Furthermore, to improve the LNA's input compression point, we utilized parasitic inductances (L_{s1}, L_{s2}) of the bonding wires and pins for emitter degradation with no chip penalty.

The image-rejecting mixer (IRMIX, which serves as the MIX block of Fig. 1) is composed of two poly-phase filters [16] and two Gilbert mixers [17], as shown in Fig. 4. One poly-phase filter is used as the RF–local-signal (RF–Lo) phase shifter, which produces two local signals from the VCO output; these are 90° phase-shifted with respect to each other and supplied as local clock signals in two phases (Lo-I and Lo-Q) to the two Gilbert mixers. The other poly-phase filter is designed so that image-frequency interference is cancelled out over a wide frequency range. The outputs

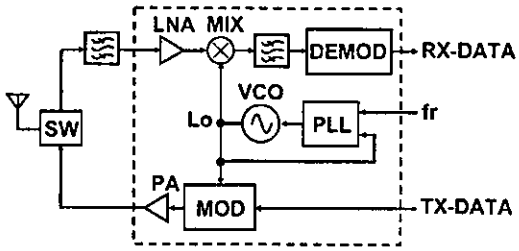

Fig. 1 Block diagram of a Bluetooth transceiver.

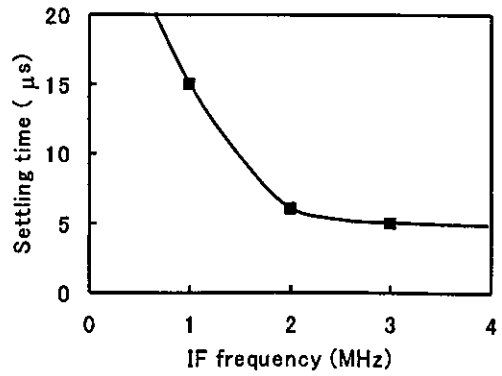

Fig. 2 Settling time for the band-pass filter.

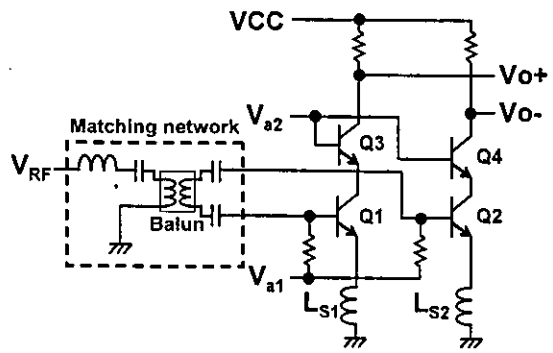

Fig. 3 The LNA circuit.

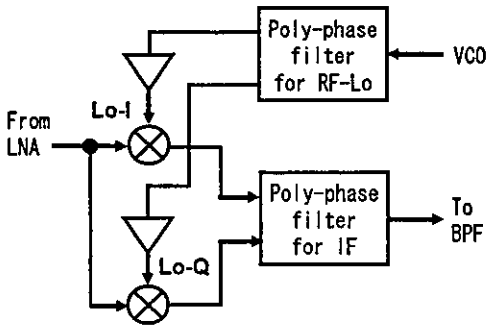

Fig. 4 Circuit diagram of IRMIX.

Table 1 LNA and MIX characteristics.

	Measurement	Simulation
Gain	17.1 dB	18.5 dB
ICP	-23.6 dBm	-24.0 dBm
NF	4.5 dB	3.9 dB
IMR@2MHz	33 dB	31.0 dB
Icc	13.3 mA	12.9 mA

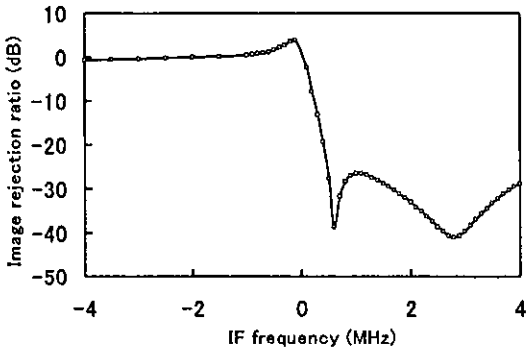

Fig. 5 Image rejection ratio of IRMIX.

of the respective mixers, shifted by 45° in the positive and negative directions, are added at the poly-phase filter.

Table 1 summarizes the results of measurement and simulation for the low-noise amplifier and image-rejecting mixer. The results are in fairly good agreement with each other thanks to the careful extraction of parasitic components from the layout. Figure 5 shows how the image-rejection characteristic varies with IF frequency. The mixer achieves a good image-rejection ratio, well below the −20 dB minimum required by the Bluetooth standard.

2.1.2 Band-Pass Filter with Variable Gain Amplifier

The output of the image-rejecting mixer is input to the analog BPF via a variable gain amplifier (VGA). Compensation for the inter-symbol interference (ISI) introduced by this analog BPF is applied in the digital domain.

The gain-control circuit for the VGA is shown in Fig. 6. It is very important that the AGC settle within 6 symbol periods (= 6 μs), because the Bluetooth standard requires that

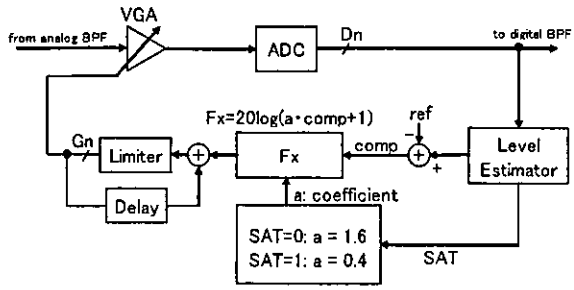

Fig. 6 The AGC: block diagram.

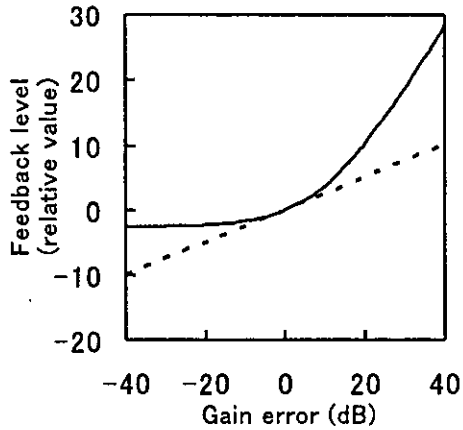

Fig. 7 The AGC: loop gain.

the transceivers have fast performance in capturing.

For high-speed control of the gain, we use a logarithmic error function in the feedback loop. The AGC consists of a level estimator that calculates the average output level of the ADC, a subtractor that subtracts the target level (ref) from the result, a logarithmic error function (Fx), 20log(a*comp+1), an integrator that includes a limiter, and a selector that selects the appropriate gain tap of the VGA.

Casting the error function Fx in a logarithmic form gives the AGC a very large initial loop gain, at which point the gain error of the AGC is large. However, the loop gain of the AGC becomes small after its activation, because the weight of the logarithm is very small when the error is around zero. The loop gain is shown in Fig. 7. Results for both the proposed method (solid curve) and the conventional logarithmic feedback method (dashed line) are given for comparison [19]. We see that the new AGC has fast convergence and its operating point remains stable after convergence. The VGA is controllable through a range of 60 dB, with a gain step of 2 dB. After convergence, the level estimator controls the signal SAT to reduce the gain, a, of the logarithmic error function to 1/4; this prevents further fluctuations in the gain of the VGA.

Figure 8 shows the result of simulation for settling of the convergence process of the AGC, as obtained by using the Advanced Design System (Agilent Technologies). To cover the range of AGC settling time, we performed six sim-

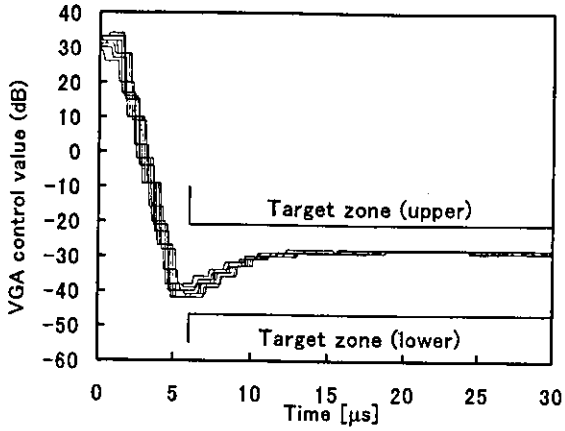

Fig. 8 The AGC: settling time. (result of simulation)

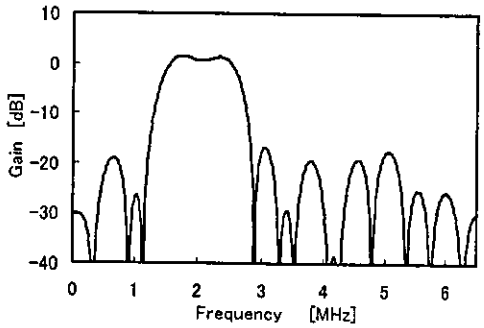

Fig. 9 Frequency characteristic of the digital filter.

ulation runs, with the received signals at maximum (worst-case) input level and in six different phases. After the start of transmission, convergence of the gain to within the allowed tolerance around the target level took no more than six symbol periods. Since the Bluetooth standard specifies that a signal being transmitted take two symbol periods to raise and then have a four-symbol preamble, the settling speed of the proposed AGC is adequate.

2.1.3 Demodulator

The channel-selection filter, realized as an FIR filter, is followed by a PLL-based demodulator with limiters. The frequency characteristic of the digital channel-selection filter is shown in Fig. 9. The frequency response of the filter is carefully designed to obtain a good eye-opening at the output of the demodulator.

Figure 10 shows the structure of the PLL-based demodulator. It consists of an image rejecter, which includes a Hilbert-transform-based 90° phase shifter, a digital loop filter, a numerically controlled oscillator (NCO), and a low-pass filter (LPF). The loop filter used was a lag-lead type that includes an integrator and multipliers. The coefficient Ka selects a period of 2-MHz for the NCO. The advantage of the PLL-based demodulator is that it is inherently robust against input-level fluctuation, since its operation is solely

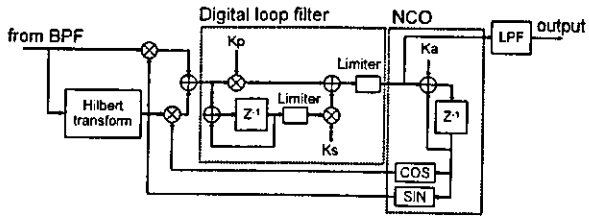

Fig. 10 Limiter-equipped PLL demodulator.

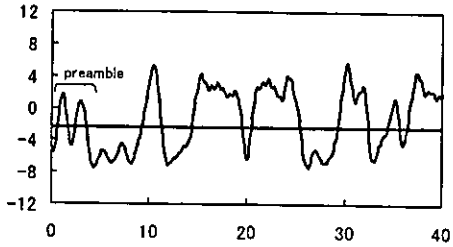

Fig. 11 Demodulator performance. (result of simulation)

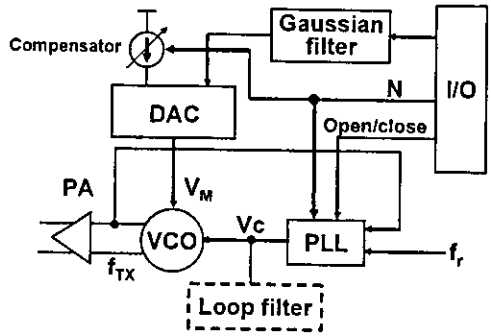

Fig. 12 Transmitter including a modulation-index compensator.

based on the phase information in the input signal.

However, we have to be careful to avoid side-locking of the PLL, i.e., locking to higher harmonics of the carrier frequency. The two limiters in the loop prevent this. Figure 11 shows the result of simulated demodulation of a signal with a 50-kHz frequency offset in the presence of interference at 2 MHz. As the figure shows, the transmitted four-symbol preamble ("1, 0, 1, 0") is recovered correctly.

2.2 Transmitter

2.2.1 Transmitter Architecture

The Bluetooth standard specifies that the transmitter use GFSK (Gaussian frequency-shift keying) to encode symbols. This consists of a Gaussian filter for waveform shaping and an FM modulator. To achieve a small chip area, we require a simple FM-modulator architecture. Here, we chose the open-loop modulation architecture shown in Fig. 12. An open/close signal selects set-up-mode or transmitting-mode operation for the PLL (operating and non-operating, respectively). The VCO used here has two control terminals and

operates in the range around 2.4 GHz. One control terminal, V_C, is used to tune the carrier frequency. The output signal from the DAC, that is, the modulated signal, is applied to the other control terminal, V_M; the GFSK-modulated signal for transmission is thus produced.

However, one result of this architecture is that the modulation-index of the transmitter varies over the Bluetooth frequency range. The sensitivity of the VCO to modulation is described by

$$\frac{G_{F1}}{G_{F2}} = \left(\frac{f0 \pm \Delta f}{f0}\right)^3, \quad (1)$$

where f0 is the central carrier frequency and Δf is the distance of the channel in use from f0. The Bluetooth specification creates a ± 5% variation in carrier frequency. Changes of modulation index with carrier frequency thus reach half of the ± 11% variation allowed by the Bluetooth specification, i.e., frequency shifts produced by modulation must be in the range between 140 and 175 kHz from the carrier. Furthermore, frequency gain of voltage-to-frequency conversion by the VCO varies by several percent with temperature; we thus need to minimize the variation contributed by the transmitting architecture.

Here, we developed a new compensation technique to reduce the variation in modulation index across the transmission bandwidth. A variable reference current is applied to a DAC, defining the maximum output voltage. The current source is controlled by the PLL synthesizer's division ratio, N. The DAC takes a 5-bit input from the Gaussian filter, which controls the internal source relative to the reference current. The operating clock for the DAC runs at 6.5 MHz. The key compensatory technique is selection of the reference current of the DAC by the division ratio N of the PLL synthesizer.

This technique reduces the results for modulation-index variation with carrier frequency by one-third, so that final variation is less than ±1.8% of the value allowed by Bluetooth.

2.2.2 VCO

The VCO is the most important circuit component for good transceiver performance. The VCO must have a phase-noise level below −120 dBc/Hz and be immune to variation in VCC.

Figure 13 shows the VCO circuit. It has two control terminals, V_C, V_M and tanks tapped by capacitors are used to provide the same GND plane for both control-terminal voltages. A single negative capacitor (C_5) ensures that the oscillation frequency of the VCO is not decreased by the parasitic capacitance of the inductor.

The transistors, Q_1 and Q_2, are in a cross-coupled structure, creating a negative conductance. Fluctuation of the bias levels, V_{b1} and V_{b2}, leads to variation of the parasitic capacitances of the transistors, which in turn leads to variation of the oscillation frequency. Avoiding this by ensuring

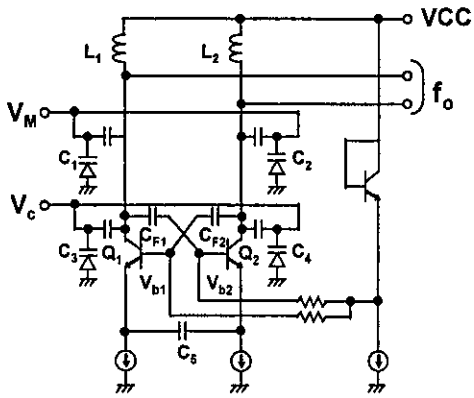

Fig. 13 The VCO.

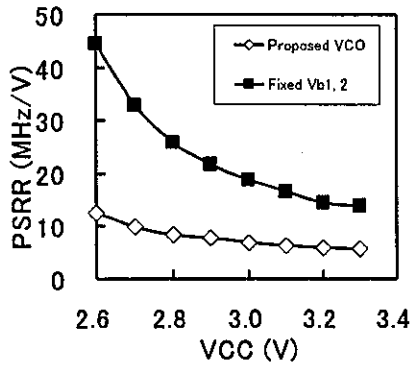

Fig. 14 The VCO: result of PSRR measurement.

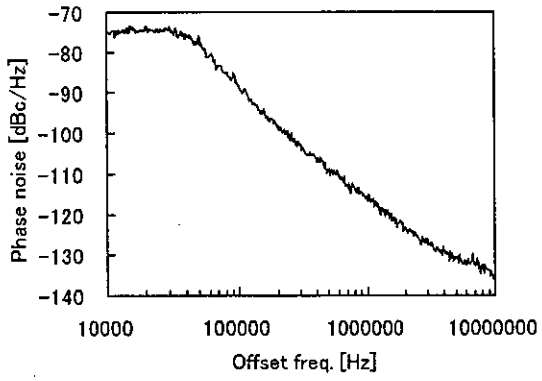

Fig. 15 The VCO: result of phase-noise measurement.

that V_{b1} and V_{b2} are fixed is not appropriate, since the voltages between the bases and collectors of Q_1 and Q_2 will still vary with VCC. This leads to fluctuations in the frequency of oscillation such that the power-supply rejection ratio (PSRR) for oscillation frequency is poor.

The biasing method we propose avoids both problems. As we see in Fig. 13, biasing voltages V_{b1} and V_{b2} are derived from VCC, so that the voltages between the bases and collectors of Q_1 and Q_2 are kept stable and are less dependent on variations in VCC.

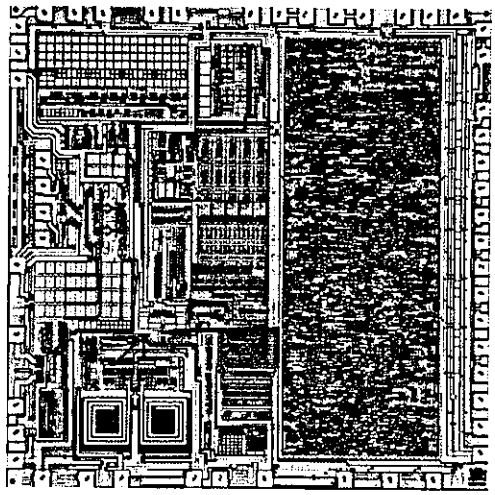

Fig. 16 Chip photograph.

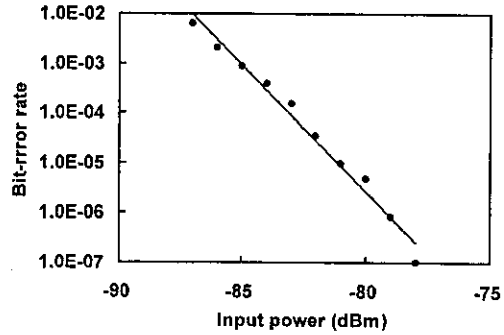

Fig. 17 Measured minimum input sensing level of the transceiver.

Figure 14 shows the results of PSRR measurement for this VCO and one in which fixed biasing is applied. The proposed method is highly effective. Results for phase-noise are shown in Fig. 15. A good phase-noise characteristic is attained, with variation of only −128 dBc/Hz at a 3-MHz offset frequency.

3. Transceiver Measurement Results

We fabricated the new Bluetooth transceiver by using four-metal, 0.35-μm BiCMOS technology. The chip size is 3.0 × 3.0 mm^2, and a photo of the chip is given as Fig. 16.

Figure 17 shows the measured result for minimum input sensitivity, where the receiver achieves the low value of −85 dBm at the Bluetooth-specified maximum bit-error rate. Interference performance measurement results are summarized in Table 2. All of the requirements of the Bluetooth standard are satisfied with margins suitable for production, thanks to the receiver's digital channel-selection filter. Results of test-chip evaluation are summarized in Table 3.

Results for chip area are compared with those of circuits presented at previous the ISSC Conferences in Table 4. Until now, Zeiji et al.'s analog circuit [7] was the smallest of Bluetooth transceivers. The reported RF area is 5.5 mm^2; this was achieved with a 0.18-μm CMOS process. The RF and IF analog modules of this work take up a total area of only 3.9 mm^2, and were implemented by using a 0.35-μm BiCMOS process. This demonstrates the effectiveness of our digital architecture in terms of saving on the overall chip size.

Table 2 Measured results for interference performance.

Interference frequency	Bluetooth Specification	C/I (dB)
IF+3MHz	-40	-43.6
IF+3MHz	-40	-43.6
IF+2MHz	-30	-34.6
IF+1MHz	0	-3.2
Co	11	9.3
IF-1MHz	0	-4.7
IF-2MHz	-30	-36.6
Image-1MHz	-20	-32.3
Image	-9	-22.6
Image+1MHz	-20	-40.3

*Image frequency is offset by −4 MHz from the carrier.

Table 3 Summary of measured results.

Item		Result
Supply voltage		2.7 V
Current	Tx	35 mA
	Rx	45 mA
Actual sensitivity		-85 dBm
VCO phase-noise level at 3-MHz offset frequency		-128 dBc/Hz
Output power level		+4 dBm
Modulation index variation		±1.8%
Frequency drift (5 packets)		20 kHz
Initial frequency offset		3.4 kHz
Eye-opening ratio		0.84

Table 4 Chip-area comparison.

	RF area/chip size (mm^2)	Technology
This work	3.9/9.0	0.35-um BiCMOS
Ref [8]	? /19.5	0.35-um BiCMOS
Ref [5]	? /16.9	0.5-um BiCMOS
Ref [7]	5.5 (4*)/ -	0.18-um CMOS
Ref [14]	5.9/ -	0.18-um CMOS

* This area is taken up by the analog circuits alone.

4. Conclusion

We have developed a small-chip-area transceiver IC for Bluetooth. Fabricated with 0.35-μm BiCMOS technol-